https://doi.org/10.31436/iiumej.v26i3.3606

CORROSION EVALUATION ON FLY ASH AND SILICA FUME CONCRETE USING NDT METHODS

AHMAD ZAKI[1,2*], FERDI ARDIAN SYAH[1], SRI ATMAJA P. ROSYIDI[1]
KHARISMA WIRA NINDHITA[2], ZAINAH IBRAHIM[3]

[1]*Department of Civil Engineering, Faculty of Engineering, Universitas Muhammadiyah Yogyakarta, Indonesia*
[2]*Magister of Civil Engineering, Faculty of Engineering, Universitas Muhammadiyah Yogyakarta, Indonesia*
[3]*Department of Civil Engineering, Faculty of Engineering, University of Malaya, Malaysia*

**Corresponding author: ahmad.zaki@umy.ac.id*

(Received: 3 February 2025; Accepted: 7 March 2025; Published online: 9 September 2025)

ABSTRACT: Corrosion of reinforced concrete is a major problem that can weaken a structure and even cause it to fail. On a macro level, this affects the safety and durability of important structures like bridges, buildings, and roads, leading to high repair costs and safety risks. On a micro level, corrosion begins with chemical reactions between steel and concrete, resulting in cracks, surface damage, and weakening of the concrete, which in turn reduces its strength and performance. This study examines the effects of using industrial waste, namely fly ash (FA) and silica fume (SF), as alternative solutions to improve reinforced concrete's corrosion resistance and mechanical performance. Concrete is made with FA substitutions of 10%, 20%, and 30% of the cement weight, and SF of 5%, 10%, and 15%, respectively. Compressive strength and flexural tests were performed to evaluate the mechanical properties, and corrosion analysis was conducted through non-destructive testing (NDT) to assess the corrosion resistance. Corrosion testing was carried out with accelerated corrosion for 48, 96, and 168 hours. Microstructural analysis using SEM was also performed to observe the effect of corrosion on the concrete. The results showed that the compressive strength of normal concrete and concrete with FA and SF decreased from 37 MPa to 25-35 MPa, respectively. The flexural strength of normal concrete and concrete with FA and SF decreased from 13 to 2 MPa due to increased corrosion rates, respectively. However, the normal concrete's resistivity value and impact echo frequency were lower than those of FA- and SF-mixed concrete. Significant resistivity values and frequency reductions were observed after corrosion, with V3 specimens (30% FA and 15% SF) showing the best corrosion durability performance.

ABSTRAK: Hakisan konkrit bertetulang merupakan masalah utama yang boleh melemahkan struktur dan bahkan menyebabkan kegagalan keseluruhan. Pada peringkat makro, ia menjejaskan keselamatan dan ketahanan struktur penting seperti jambatan, bangunan, dan jalan raya, sekali gus membawa kepada kos pembaikan yang tinggi serta risiko keselamatan. Pada peringkat mikro, hakisan bermula dengan tindak balas kimia antara keluli dan konkrit, menyebabkan rekahan, kerosakan permukaan, dan kelemahan pada konkrit, yang akhirnya mengurangkan kekuatan dan prestasinya. Kajian ini meneliti kesan penggunaan sisa industri iaitu abu terbang (FA) dan wap silika (SF) sebagai penyelesaian alternatif untuk meningkatkan rintangan hakisan dan prestasi mekanikal konkrit bertetulang. Konkrit dihasilkan dengan penggantian FA sebanyak 10%, 20%, dan 30% daripada berat simen serta SF sebanyak 5%, 10%, dan 15%. Ujian kekuatan mampatan dan lenturan dijalankan bagi menilai sifat mekanikal, manakala analisis hakisan melalui kaedah tanpa musnah (NDT) digunakan untuk menilai rintangan hakisan. Ujian hakisan dijalankan menggunakan kaedah

hakisan dipercepat selama 48, 96, dan 168 jam. Analisis mikrostruktur menggunakan SEM turut dilakukan bagi memerhati kesan hakisan terhadap konkrit. Hasil kajian menunjukkan bahawa kekuatan mampatan konkrit normal serta konkrit dengan FA dan SF menurun daripada 37 MPa kepada 25–35 MPa. Kekuatan lenturan konkrit normal serta konkrit dengan FA dan SF juga menurun daripada 13 MPa kepada 2 MPa apabila kadar hakisan meningkat. Namun begitu, nilai rintangan dan frekuensi gema hentakan bagi konkrit normal adalah lebih rendah berbanding konkrit yang dicampur FA dan SF. Nilai rintangan serta pengurangan frekuensi yang ketara diperhatikan selepas hakisan, dengan spesimen V3 (30% FA dan 15% SF) menunjukkan prestasi ketahanan hakisan yang terbaik.

KEYWORDS: *Fly Ash, Silica Fume, Concrete, Corrosion, NDT*

INTRODUCTION

Corrosion of reinforcements is one of the main causes of premature damage to reinforced-concrete (RC) structures. The corrosion process is caused by the reaction between reinforcing steel and hydroxide (OH) ions derived from the reaction between oxygen and water. This can occur because of damage to the passive layer of the rebar, known as depassivation, which is caused by the infiltration of chloride ions (Cl^-) into concrete [1-3]. Steel reinforcement has a corrosion-protective layer known as a passive film. However, this layer can be destroyed by the chloride ions or carbon reactions around the reinforcement. When the concentration of chloride ions reaches a critical threshold on the surface of the steel reinforcement, the coating passivity film is eroded, and the corrosion process occurs immediately [1]. To overcome this corrosion problem, the development and use of mixed cement has begun to develop rapidly in the construction industry, mainly owing to the consideration of cost savings, energy savings, environmental protection, and resource conservation. Fly ash, a silica material obtained from various thermal power plants, is considered a cement material for concrete [4]. In general, there are two types of additives: mineral and chemical. The better the characteristics of the additives used, the better the concrete will be produced.

Fly ash (FA) is a very fine coal combustion residue. Fly ash has similar physical properties to cement, namely, the fineness of the grains and the chemical content in the form of silica [5]. The second mineral additive is Silica Fume (SF). Silica fume is a very fine pozzolan material composed mostly of amorphous silica produced by electric arc furnaces as a byproduct of silicon production. Silica fumes contain silica compounds and have very fine grains up to 100 times smaller than cement grains. Saraswathy et al. [4] examined the effects of activated fly ash on concrete's corrosion resistance and strength. Concrete with 10%, 20%, 30%, and 40% activated FA (chemical and thermal activation) was tested for compressive strength at 7, 14, 28, and 90 days. The results showed that chemical activation was more effective in improving the corrosion resistance and strength of concrete, with the replacement of 20%-30% of activated FA improving the corrosion resistance of concrete. Zaki et al. [2] examined the effect of corrosion on palm shell concrete and mask fibers using non-destructive testing (NDT), i.e., resistivity and impact echo methods. Concrete underwent accelerated corrosion with a 5% NaCl solution and a DC power supply. The results showed that corrosion decreases the strength and durability of concrete, and the NDT method effectively detects corrosion in concrete.

Several studies have shown that the addition of pozzolan additives to concrete, such as FA and SF, increases the sealing properties against water penetration. The use of FA can modify the characteristics of fresh and hard concrete by improving the fatigue level, strength, and abrasion resistance [6]. According to Saraswathy et al. [4], a concrete mix that uses FA and SF as a substitute material for cement produces good concrete strength compared to normal concrete. Despite growing interest in sustainable concrete technologies, limited research has

been conducted on evaluating corroded concrete incorporating supplementary cementitious materials (SCMs) like FA and SF, mainly through NDT methods. Most existing studies focus on the mechanical strength development of FA/SF concrete [5, 6], corrosion resistance improvements due to pozzolanic reactions [4, 5], chloride permeability and durability metrics using destructive tests (DT) [2, 5], and NDT methods (i.e., ultrasonic pulse velocity (UPV), rebound hammer, ground-penetrating radar (GPR), electrical resistivity) on ordinary Portland cement (OPC)-based concrete, often without incorporating SCMs.

This study achieved the maximum concrete strength by replacing 20%-30% of the cement. Therefore, it is essential to conduct further research with cement replacement of fly ash by 10%, 20%, and 30%, and silica fume by 5%, 10%, and 15%, respectively. Variations were selected based on several references' optimum FA and SF values. Thus, the strength ratio between normal concrete and mixed concrete improves when the composition of fly ash and silica fume improves. In addition, this research also reviews corrosion detection using the NDT method with resistivity and impact echo tools, which can be used as reference parameters when checking structures made from fly ash and silica fume, especially before and after corrosion. This research also examines the influence of corrosion on the mechanical properties of concrete mixed with fly ash and silica fume.

RESEARCH METHODS

2.1. Materials

This research was conducted at the Civil Engineering Construction Materials Laboratory, Universitas Muhammadiyah Yogyakarta. The fine aggregate material used in this study originated from the Progo River, whereas the coarse aggregate was from Clereng, Yogyakarta. The test specimen was made using Portland Composite Cement (PCC) from Dynamix with Ø12 mm reinforced iron with a length of 60 cm. The mold of the specimen was 50 cm × 10 cm × 10 cm, according to the size of the specimen to be made. The fly ash material was obtained from Cilacap PLTU, whereas the silica fume was obtained from PT. Sika Indonesia. The laboratory test results are presented in Table 1. Figure 1 shows the sieve analysis chart.

Table 1. Fine and coarse aggregate test data

Types of Testing	Fine Aggregate Value	Coarse Aggregate Value	Unit
Fine modulus of grain	2.435	-	-
Bulk specific gravity	1.837	2.642	-
The specific gravity of saturated dry	2.243	2.707	-
Specific gravity apparent	3.094	2.826	-
Water absorption	22.16	2.46	%
Sludge rate	1.00	1.00	%
Abrasion	-	15.75	%

https://doi.org/10.31436/iiumej.v26i3.3606

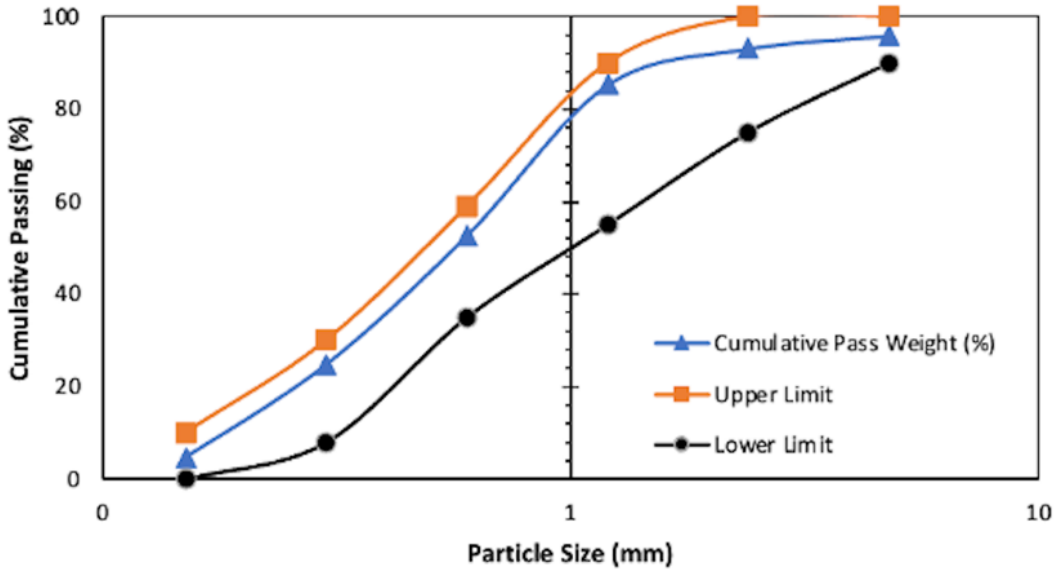

Figure 1. Cumulative passing (%)

2.2. Mix Design Concrete

Concrete mix planning using ACI 211.1-91 concerns procedures for maintaining proportions for normal concrete production with a planned concrete quality of 30 MPa [7]. Proportions of fly ash (FA) of 10%, 20%, and 30%, and silica fume (SF) of 5%, 10%, and 15% were added, respectively. Fly ash proportions of 10%, 20%, and 30% and silica fume proportions of 5%, 10%, and 15% were selected to evaluate their individual systematic and combined effects on concrete properties, including strength, durability, and workability. These ranges fall within standard practice and allow for optimizing the pozzolanic reaction, cost-effectiveness, and sustainability while balancing early and long-term performance. The mix design proportions per m³ are shown in Table 2. NC is normal concrete, V1 is concrete with 10% FA and 5% SF, V2 is concrete with 20% FA and 10% SF, and V3 is concrete with 30% FA and 15% SF.

Table 2. Proportion mix design per m^3

Material	TOTAL				Unit
	NC	V1	V2	V3	
Water	205	205	205	205	liter
Cement	484.21	411.44	338.84	266.23	kg
Sand	641.52	641.52	641.52	641.52	kg
Gravel	984.75	984.75	984.75	984.75	kg
Fly Ash	-	48.40	96.81	145.21	kg
Silica Fume	-	24.20	48.40	72.61	kg

2.3. Specimens Fabrication

The test specimen was in a beam (50 × 10 × 10 cm) and cylindrical form (30 × 15 cm), as shown in Figure 2. The main reinforcement size was Ø12 mm. A small cable was attached to the end of the reinforcement as a channel for accelerating concrete corrosion using a DC power supply. The test specimen was made based on a mixture proportion of fly ash (10%, 20%, and 30%) and silica fume (5%, 10%, and 15%). After the slump test, the concrete mixture was

https://doi.org/10.31436/iiumej.v26i3.3606

poured into the formwork until it was full and dense so air cavities did not form. The concrete was left to harden for 24 hours and then removed from the formwork.

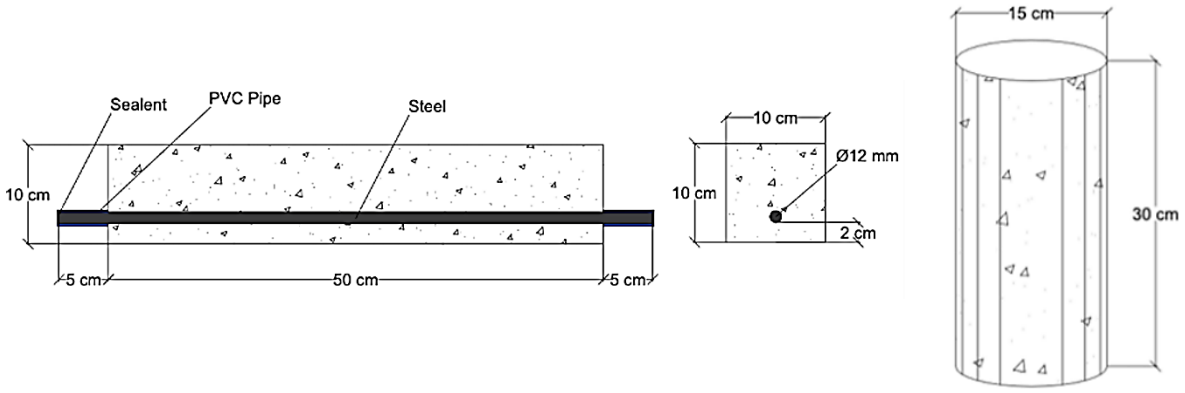

(a) (b)

Figure 2. Specimen schematic (a) beam specimen and (b) cylinder specimen

This test was performed based on ACI 211.1-91 [7] to determine the concrete's viscosity. The slump test results were expressed in centimeters using an Abrams cone tool, a fist stick, and a meter. This study was planned to have a slump value of 25-100 mm. The test result slumps are shown in Table 3. Curing in concrete is a method used to maintain temperature stability, prevent moisture changes inside and outside the concrete, and help speed up the hydration process of the concrete. In this study, curing was performed by soaking the specimens for 28 days.

Table 3. Test scores slump

	Variations		Slump Value (cm)
	Fly Ash (%)	Silica Fume (%)	
NC	0	0	10
V1	10	5	9.5
V2	20	10	8
V3	30	15	7

2.4. Resistivity Testing

The resistivity test was performed when the specimen was 28 days old. The test was performed before and after the corrosion acceleration process to compare the test results based on AASHTO TP95-14 [8]. To obtain more complete and accurate data, the resistivity measurement tool employs the four-point probe method, which is performed three times at each point, ensuring that the data obtained is comprehensive and accurate. The details of the point division in which the resistivity test was carried out are shown in Figure 3. The sides are divided into four areas: the upper side, directly connected by the cable; the lower side; the right side; and the left side. Point division is used to obtain accurate and even results, so the average is obtained.

https://doi.org/10.31436/iiumej.v26i3.3606

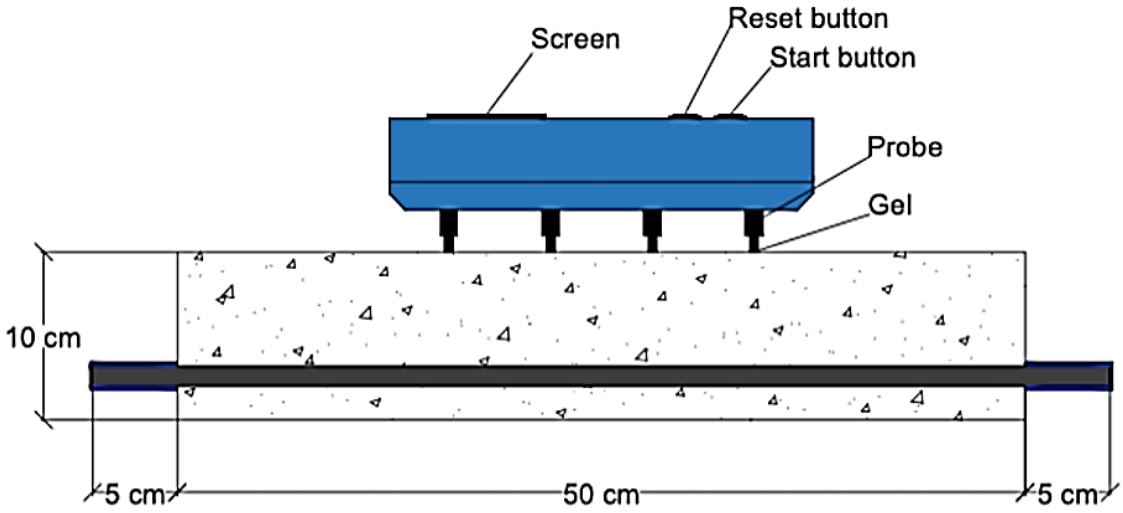

Figure 3. Testing illustration of resistivity

2.5. Impact Echo Testing

Impact-echo testing was performed when the specimen was 28 days old. The test was performed before and after the corrosion acceleration process to compare the test results. The impact-echo method was used to detect defects in concrete based on ASTM C1383 [9]. This is based on monitoring surface movements due to short-term mechanical impacts. The concrete is tapped several times using an impact echo test tool, and the sensor receives signals at a predetermined distance between it and the point of impact. Figure 4 illustrates the impact echo test. Impact echo testing was performed with two sensors at 5, 10, 15, and 20 cm hit points. The details of the impact echo test at each distance are shown in Figure 4.

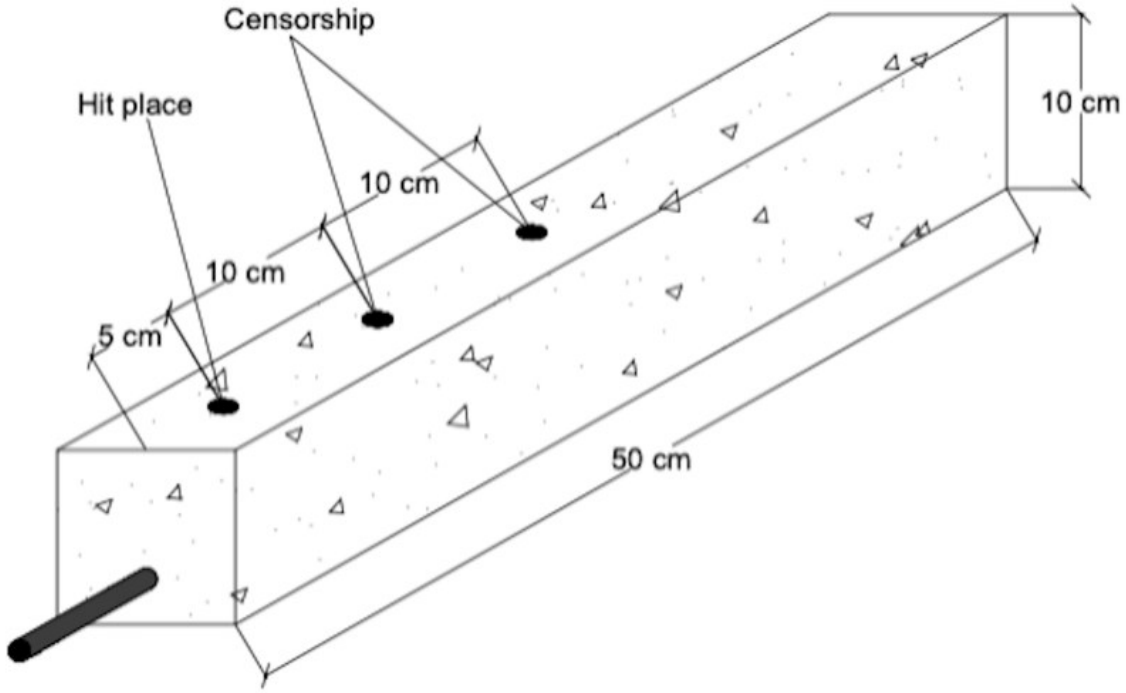

Figure 4. Impact echo test illustration

https://doi.org/10.31436/iiumej.v26i3.3606

2.6. Accelerated Steel Corrosion

In this test, the specimen's corrosion acceleration is required owing to the very long natural corrosion process based on ASTM STP866-EB [10]. The steel reinforcement on concrete is corroded using a DC power supply tool to speed up the corrosion process and adjust the duration and use of the electric current as needed. The reinforcing steel was connected to the positive (+) pole as its anode, and the other reinforcing steel was attached to the negative pole (-) as the cathode [11]. The solution had a salinity of 5% and a corrosion percentage of 20% using a DC power supply with a current of 5 A. The water level is 12.5 cm from the bottom of the container. The salinity of the salt solution was maintained at 5%. Before the concrete was immersed, the concrete reinforcement was wired on one side to connect to the positive pole of the DC power supply tool. The salt solution was then soaked into the concrete and reinforcement parts. The reinforcement used on the negative pole was completely submerged. The corrosion acceleration scheme is illustrated in Figure 5.

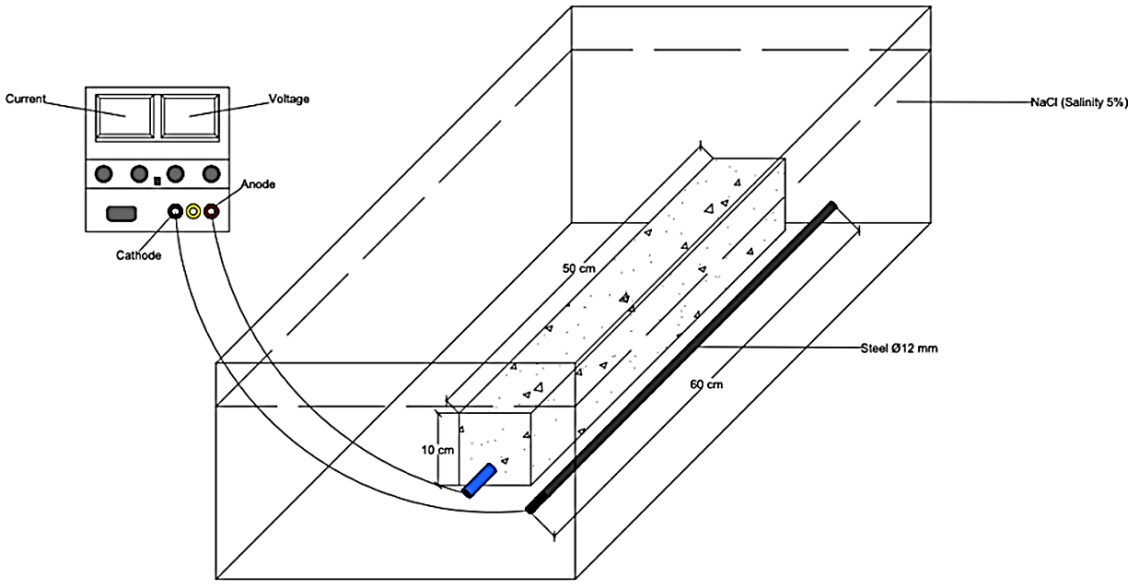

Figure 5. Corrosion acceleration testing scheme

2.7. Concrete Mechanical Testing

Compressive strength testing was performed at the Laboratory of Civil Engineering Structures and Construction Materials, Universitas Muhammadiyah Yogyakarta. This test was performed on 28-day-old cured cylindrical concrete. A Universal Testing Machine is a tool that determines the compressive strength of a test specimen in a concrete mixture using fly ash and silica fume. The compressive strength test scheme is illustrated in Figure 6 (a). The bending strength of concrete was tested using a Universal Testing Machine after the corrosion process was completed. Concrete bending strength testing was performed at the Laboratory of Structure and Construction Materials, Civil Engineering, Universitas Muhammadiyah Yogyakarta. The test was carried out with two loading points in the middle of the beam span and a distance of 5 cm between the pedestal and the edge of the beam. This test aimed to determine the flexural strength of the corroded beams at each percentage of fly ash and silica fume. The flexural strength test scheme is illustrated in Figure 6 (b).

https://doi.org/10.31436/iiumej.v26i3.3606

(a) (b)

Figure 6. (a) Compressive strength testing and (b) Flexural strength testing

RESULTS AND DISCUSSIONS

3.1. Compressive Strength

The results of the compressive strength tests are shown in Figure 7. Fly ash (FA) and silica fume (SF) influence the compressive strength of concrete by enhancing the pozzolanic reaction and improving the microstructure. FA contributes to long-term strength gain through gradual pozzolanic activity. At the same time, SF significantly increases early and later-age strength by filling microvoids and forming additional calcium silicate hydrate (C-S-H), resulting in a denser and stronger concrete matrix. Compressive strength of concrete is planned for Mix Design at 30 MPa. Meanwhile, after testing based on Table 5, the actual compressive strength of concrete was found to be regular concrete without any additives or mixtures, with an average compressive strength of 37.59 MPa. Concrete with 10% FA and 5% SF variations produces an average compressive strength value of 35.10 MPa. The concrete variations of FA 20% and SF 10% show an average compressive strength value of 33.80 MPa. The compressive strengths of the 30% FA and 15% SF concrete yielded an average of 27.44 MPa. Several factors affect compressive strength: the compaction process, which is not optimal, and the material factor, Pozzolan [12]. Adding SF tends to result in higher water absorption, so the workability is low (as shown in the slump value results), making it difficult for fresh concrete to drain correctly into the mold.

https://doi.org/10.31436/iiumej.v26i3.3606

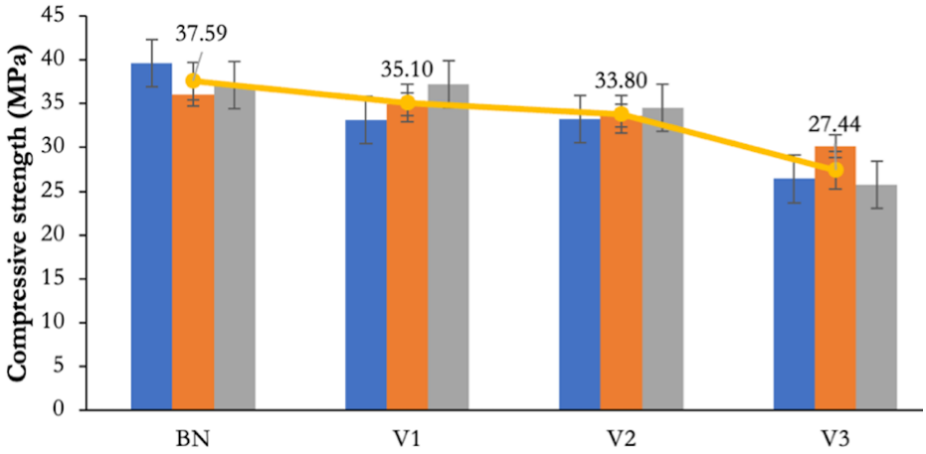

Figure 7. Results of the concrete compressive strength test

The decrease in compressive strength, along with the increase in cement replacement with FA and SF, is due to fly ash having a high silica content, and silica fume causes a decrease in the workability of concrete [13]. The specimen was monitored after testing for compressive strength to observe the crack pattern and determine the behavior of each concrete mixture when subjected to an axial load. According to SNI 1974:2011 [14], there are five types of concrete cracking patterns: cone collapse, cone and split fracture, cone and slide failure, sliding fracture, and vertical-axis parallel fracture. The crack pattern of the specimen is shown in Figs. 8 to 10. FA and SF refine the pore structure and improve the bonding within the matrix, leading to higher tensile strength and reduced crack width or spacing while influencing drying shrinkage and thermal properties, which can alter how and where cracks form compared to normal concrete. In addition, higher amounts of SF typically lead to a denser and stronger matrix, resulting in finer, narrower cracks, while increasing FA content improves long-term strength and reduces thermal cracking. Still, excessive FA may delay early strength gain, potentially leading to wider or more irregular cracking at early ages if not properly cured.

Figure 8 shows the collapse pattern in cylindrical concrete with variations of 10% FA and 5% SF. Figs. 8(a), (b), and (c) show different crack patterns. Figure 8(a) and (b) show the same crack pattern, namely cone and shear, whereas Figure 8(c) shows the shear crack pattern. The failure mechanism in concrete, particularly the development of cone cracking and shearing, is influenced by several factors, including aggregate distribution, interfacial transition zones (ITZ), and localized stress concentrations. Uneven aggregate size can lead to non-uniform stress distribution within the matrix, but this alone does not comprehensively explain the observed failure modes. Instead, cone cracking is typically initiated by point loading or high compressive stress beneath loading points, where tensile stresses radiate outward. Figure 9 shows the collapse pattern in cylindrical concrete with 20% FA and 10% SF. Figure 9(a) shows a sliding crack pattern, Figure 9(b) shows a columnar crack pattern, and Figure 9(c) shows a cone crack pattern. These different cracking patterns were caused by uneven or poorly adhered capping of the concrete surface, resulting in varying tension concentrations in each test piece. Figure 10 shows the collapse pattern of the cylindrical concrete with 30% FA and 15% SF. Figure 10 (a), (b), and (c) show similar crack patterns, namely shear crack patterns. A shear crack pattern occurs in concrete with low compressive strength and is ductile. Shear crack patterns in concrete have significant implications on structural performance, as they indicate potential failure in the load transfer mechanism, particularly in beams and structural members subjected to transverse loads. These cracks can reduce the stiffness, load-bearing capacity, and

https://doi.org/10.31436/iiumej.v26i3.3606

overall ductility of the structure, potentially leading to premature failure if not adequately addressed through adequate design, reinforcement, or material modification.

(a) (b) (c)

Figure 8. Concrete crack pattern with FA 10% and SF 5%

(a) (b) (c)

Figure 9. Concrete cracking pattern FA 20% and SF 10%

https://doi.org/10.31436/iiumej.v26i3.3606

(a) (b) (c)

Figure 10. Concrete cracking pattern FA 30% and SF 15%

3.2. Corrosion Acceleration Results

Corrosion testing was performed after 28 days of curing. The specimens were subjected to accelerated corrosion for 48, 96, and 168 h. The corrosion acceleration process was carried out by immersing the specimen in a NaCl solution with 5% water volume in a Styrofoam box. Meanwhile, a DC power supply was used to provide an electric current to the concrete reinforcement so that the corrosion acceleration process could occur. Graphs of concrete corrosion acceleration for durations of 48, 96, and 168 h are shown in Figure 11. The corrosion acceleration duration (48 h, 96 h, and 168 h) significantly affected the corrosion rates, with longer exposure times leading to higher corrosion levels due to prolonged electrochemical reactions and chloride penetration. As the duration increased, the degree of rust formation, crack development, and mass loss of reinforcement also intensified, indicating a direct correlation between exposure time and corrosion severity. The results of corrosion acceleration for 48 h show an increasing current trend that continues to increase until the end of the canal in some specimens.

In normal concrete, there is a significant increase until the 17th hour. Still, after that, there is a significant decrease, which is likely to occur because of the condition of the reinforcement that can no longer flow the current-voltage effectively to the entire reinforcement. Among the four specimens, the specimens with a mixture of FA and SF produced a lower initial and average flow than normal concrete. The best durability was observed for the V3 mixture, with an average current of 0.248 A. The results of corrosion acceleration at 96 h showed a fluctuating trend but tended to increase from start to finish. In this test, the best resistance behavior was observed in the V3 test specimen, with an average current of 0.612 A. At 168 h, the corrosion acceleration exhibited a fluctuating trend. In this test, the V1 test specimen showed the best resistance, with an average current of 1.160 A. From the overall test, it was observed that a significant current surge occurred for the V2 test specimen at a corrosion acceleration of 168

https://doi.org/10.31436/iiumej.v26i3.3606

hours, which initially showed the lowest initial current compared to the other specimens. Due to its lower current, concrete with FA and SF has a lower corrosion rate than normal concrete. A lower current indicates a weaker corrosion process. Additionally, FA and SF make the concrete denser and less permeable, limiting the penetration of chloride ions and moisture into the steel reinforcement. Their pozzolanic activity also improves the microstructure and alkalinity, enhancing protection against corrosion.

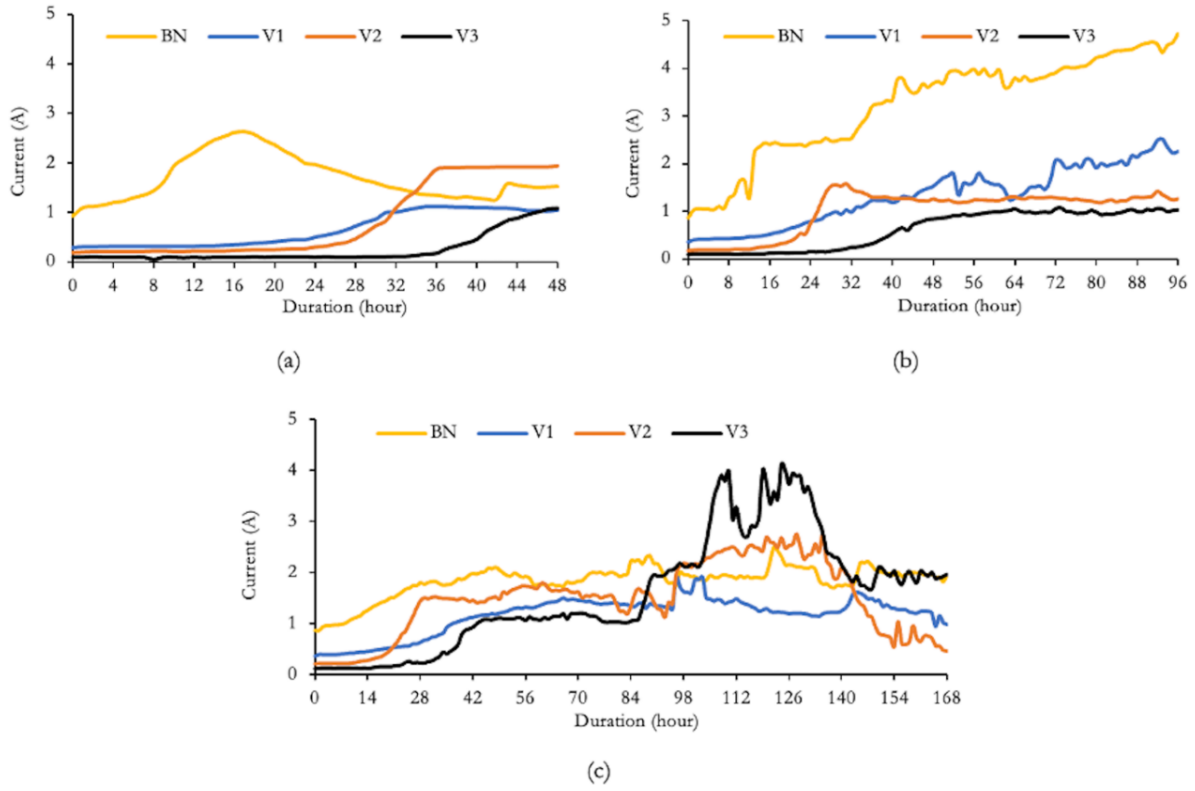

Figure 11. Corrosion acceleration graph (a) 48 h corrosion, (b) 96 h corrosion, and (c) 168 h corrosion

The results of the overall corrosion acceleration show that the initial current in the specimen with pozzolanic material was lower than that of normal concrete [15]. Subsequently, an increase in current was observed every hour owing to continuous corrosion acceleration in all specimens. At 48 h and 96 h corrosion acceleration, V3 has a low average current value. Still, at 168 h corrosion acceleration, V3 has a significant increase in current at 102 h, which is most likely due to the specimen experiencing wide cracks so that the reinforcement is not covered by concrete. After the corrosion acceleration process, cracking in each concrete specimen was observed. Cracks due to this condition can be assessed from crack patterns and width measurements. Concrete crack widths are shown in Figure 12 and Table 4.

https://doi.org/10.31436/iiumej.v26i3.3606

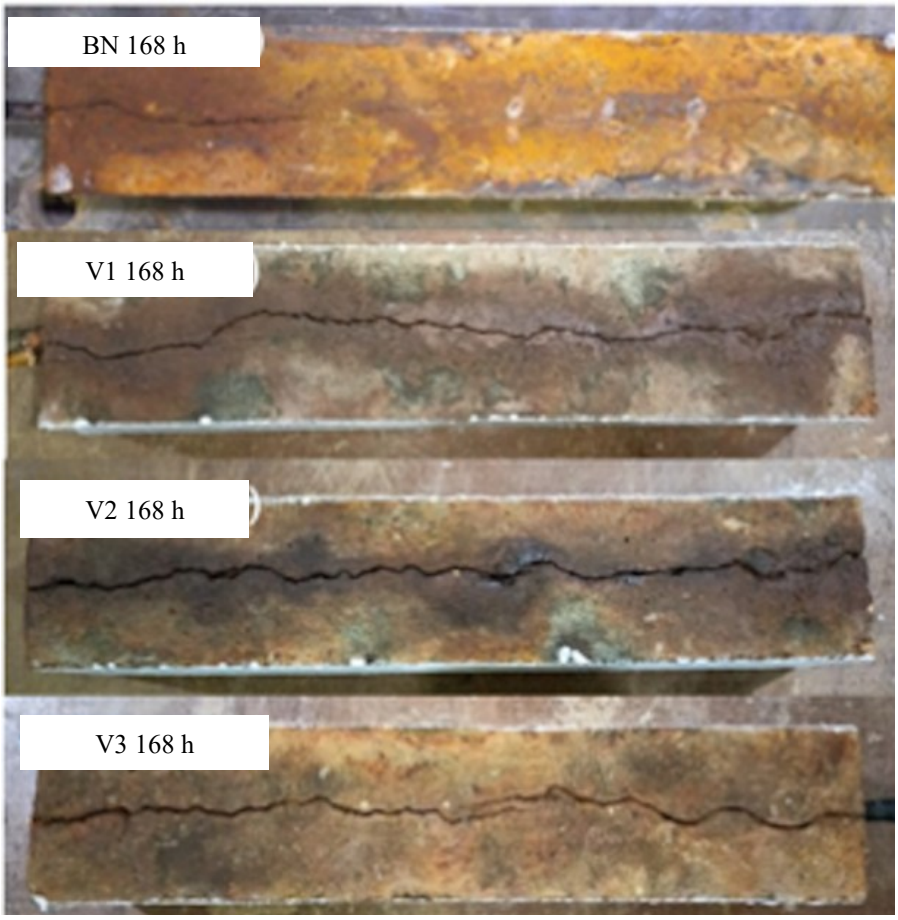

Figure 12. Concrete cracking after the acceleration process

The crack width measurements directly correlated with the corrosion rate in the concrete specimens, as wider cracks generally indicated higher corrosion activity due to the expansive pressure of rust formation. As the corrosion rate increased, the steel reinforcement expanded, causing more significant cracking that further accelerated chloride ingress, creating a feedback loop that worsened the corrosion process. Table 4 shows the width of corrosion cracking on the right and left sides of the concrete specimens. The cracking width is measured using a crack width ruler. The specimens are labeled as a, b, and c to indicate that each concrete variation has three specimens.

Table 4. Corrosion crack width

Test Specimen	Acceleration Duration (hours)	Corrosion crack width (mm)	
		Right side	Left side
BN1	48	0.60	0.30
BN2	168	6.50	0.70
BN3	96	0.75	0.40
V1a	48	0.60	0.60
V1b	96	5.00	0.85
V1c	168	0.85	0.95
V2a	48	0.60	0.60
V2b	96	0.75	0.70
V2c	168	1.40	1.30
V3a	48	0.30	0.20
V3b	96	1.10	1.40
V3c	168	1.40	3.50

https://doi.org/10.31436/iiumej.v26i3.3606

According to the observation results, a crack pattern occurred in all specimens, characterized by cracks in the longitudinal direction. Stiffness was measured on the right and left sides of the concrete. Cracks after 168 hours of corrosion duration had a comparatively larger width. This occurs because the longer the corrosion acceleration process lasts, the more rust products are produced. According to Alhawat et al. [16], the longer the corrosion process lasts, the more rust accumulates on the surface of the steel rod, and the faster the corrosion is owing to cracking, allowing a large number of electrons to move from the cathode to the anode. In addition, the durability of concrete is also an essential factor in the occurrence of cracks. The measurement results indicate that the largest cracks are most frequently observed on the right side, which is primarily characterized by cables. This is possible because the reinforcement closest to the cable has a more positive potential; therefore, electrons occur faster.

After the corrosion acceleration process and bending strength test were completed, concrete destruction was performed to determine the final rebar weight after the corrosion test. After removing the reinforcing steel from the concrete, the reinforcing iron was cleaned of rust due to the corrosion acceleration process. The reinforcing steel was weighed to determine the mass of the remaining rebar due to the corrosion process. Table 5 shows the actual mass of the concrete reinforcement due to the corrosion acceleration process. The mass loss of the reinforcement indicated that adding FA and silica fume SF effectively reduced corrosion, as specimens containing FA and SF showed significantly lower mass loss compared to normal concrete. This demonstrated their ability to enhance concrete durability, minimize chloride penetration, and better protect the embedded steel reinforcement. Table 5 shows that the actual corrosion rate of a normal concrete specimen (BN3) is 34.60%, representing a difference of 24.60% from the planned corrosion rate. Variation 1 (V1b) specimen produced an actual corrosion rate value of 18.33%, with a difference from the planned corrosion of 8.33%. In the variation 2 (V2b) specimen, the actual corrosion value was obtained at 14.17%, with a difference from the planned corrosion of 4.17%. Meanwhile, the variation 3 (V3b) specimen produced an actual corrosion value of 8.75%, different from the planned corrosion value of 1.25%.

Table 5. Percentage of rebar mass loss

Test Specimen	Corrosion Acceleration Duration (hours)	Initial Mass of Reinforcement (grams)	Mass After Corrosion (grams)	Actual Mass Loss (grams)	Actual Corrosion Rate (%)	Percentage of Mass Loss Difference (%)
BN1	48	500	454	46	9.20	4.20
BN2	168	500	287	213	42.60	27.60
BN3	96	500	327	173	34.60	24.60
V1a	48	480	461	19	3.96	1.04
V1b	96	480	392	88	18.33	8.33
V1c	168	480	344	136	28.33	13.33
V2a	48	480	457	23	4.79	0.21
V2b	96	480	412	68	14.17	4.17
V2c	168	480	332	148	30.83	15.83
V3a	48	480	472	8	1.67	3.33
V3b	96	480	438	42	8.75	1.25
V3c	168	480	374	106	22.08	7.08

From these results, it can be observed that the actual corrosion level produces different values for each variation. In addition, it is known that the corrosion rate that occurs in concrete with a mixture of FA and SF is lower than in normal concrete. This is in line with research by Gomez-Luna [17], which shows that the performance of FA and SF can prevent corrosion

https://doi.org/10.31436/iiumej.v26i3.3606

effectively. This can also be seen from the results for normal concrete (BN3), which shows the highest corrosion value. Then, in concrete variation 1 (V1b), the corrosion rate decreased by 16.27% with the addition of variation fly ash and silica fume by 10% and 5%. In variation 2 (V2b), the corrosion rate decreased by 4.17% with the addition of 20% and 10% fly ash and silica fume, respectively. Meanwhile, variation 3 (V3b) reduced the corrosion rate by 12.50%, adding FA and silica fume SF by 30% and 15%, respectively. Corrosion severely impacts the long-term durability of concrete structures by causing steel reinforcement to expand due to rust formation. This expansion leads to cracking, spalling, and a weakened bond between steel and concrete. Over time, the resulting deterioration reduces structural integrity, lowers load-bearing capacity, and shortens the structure's service life, leading to higher maintenance costs and potential safety risks.

3.3. Resistivity Results

A resistivity test was performed after the curing process was completed. The curing method involves soaking the concrete removed from the formwork in a soaking tub for 28 days. The resistivity test was performed at four points on the surface of the specimen. It is important to perform resistivity testing before and after the corrosion acceleration process to evaluate changes in the concrete's ability to resist ionic movement, which directly relates to its corrosion resistance [18]. The test results in resistivity before corrosion show a corrosion category at a very low level on test specimens with FA and SF additives, with a value range of 37-254 kΩ.cm. Normal concrete is in the low and very low corrosion category in the range of 21-37 Ω.cm. Test results show resistivity after corrosion; each specimen has a different duration of corrosion acceleration. After the specimen was corroded, there was a decrease in the resistivity, which decreased with the duration of corrosion acceleration. In specimens with FA and SF, additives were in the moderate to very low range. All normal concrete specimens were included in the moderate to low range. Resistivity is a measure of a material's ability to resist the flow of ions in an electric field. The higher the resistivity value, the better the concrete's ability to prevent corrosion. The resistivity of the test results is shown in Figure 13.

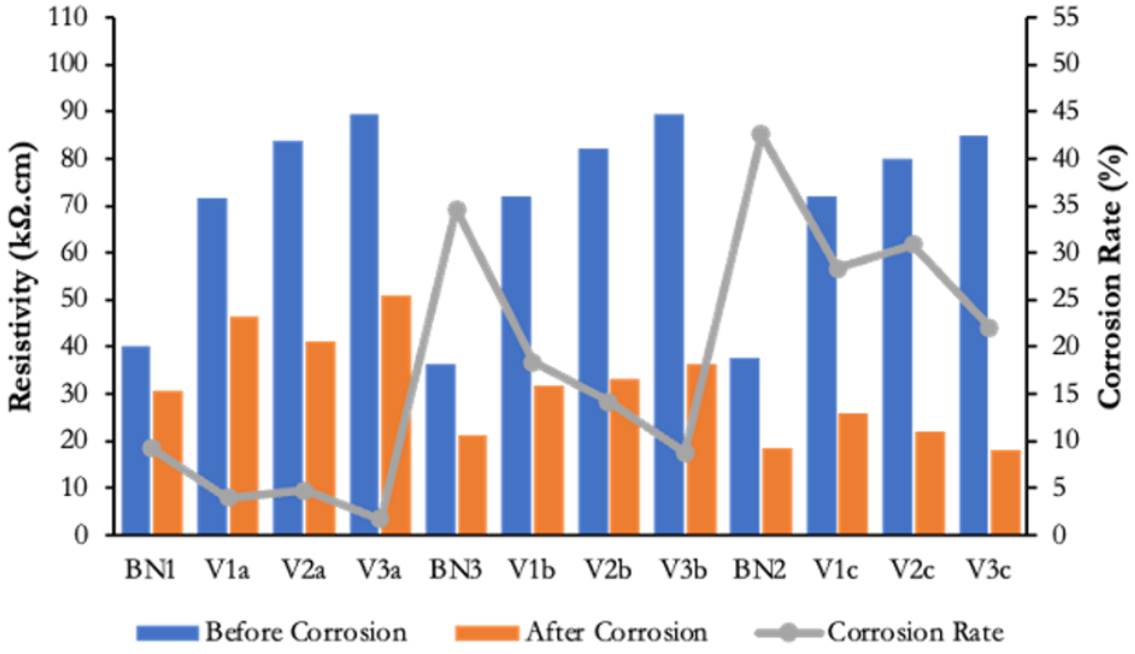

Figure 13. Relationship graph of resistivity and corrosion rate

https://doi.org/10.31436/iiumej.v26i3.3606

The environmental conditions and characteristics of the concrete mixture influence the resistivity of concrete. If the initial resistivity of concrete is high, it will provide a high current resistance, such that the corrosion level in concrete is not too high. In this study, the FA and SF specimens have higher resistivity values than normal concrete. A good corrosion resistance was observed in each FA and SF mixed concrete, and the best performance was observed in the V3 specimens. The addition of FA and SF materials can improve the bonding quality and pore structure of concrete [19]. The pore structure is the most crucial characteristic that controls the transport properties of hydrated cement paste. Therefore, with the addition of fly ash, a pozzolanic reaction can affect water permeability. Silica fume particles are smaller than cement, thus filling the space between the cement grains, which can cause the concrete to become denser and reduce water permeability [20]. The results showed that adding fly ash and silica fume can provide adequate corrosion resistance. In addition, the water-to-cement (w/c) ratio is a key factor in determining the corrosion resistance of concrete. A lower w/c ratio creates a denser, less permeable concrete, limiting the penetration of harmful agents like chloride ions and moisture. In contrast, a higher w/c ratio increases porosity, making the concrete more vulnerable to corrosion by allowing easier access for corrosive elements to the steel reinforcement.

3.4. Impact Echo Results

The impact echo test measures the quality of concrete by evaluating the propagation of stress waves through the material; reflections from internal flaws, voids, or cracks are used to assess concrete integrity, density, and thickness. The frequency is the number of vibrations occurring in one second, a unit of Hertz (Hz). The frequency obtained from the impact-echo test defines the quality of the concrete tested, and the applied frequency results are highly dependent on the distance between the specified sensors; therefore, the author tested four different sensor distances to obtain constant frequency results to make it easier to identify the impact-echo test results. Graphs of impact echo for the durations of 48 h, 96 h, and 168 h, respectively, are shown in Figure 14. From the graph displayed, it can be seen that the peak frequency shift was obtained from the impact-echo test at each corrosion percentage. This decrease in frequency is caused by a reduction in the elastic modulus of concrete owing to corrosion. The results for the peak frequency values are presented in Figure 15.

The test results showed a dominant frequency variation in each specimen before and after corrosion at different sensor positions. In this study, the specimens with a mixture of FA and SF exhibited a relatively higher frequency. The peak frequency in normal concrete ranges from 2000 Hz to 10000 Hz, whereas in the FA and SF specimens, it ranges from 5000 Hz to 18000 Hz. The highest average frequency was observed in V1, with an average value of 18726.9 Hz at a sensor distance of 10 cm. Meanwhile, normal concrete exhibited the highest average frequency value. Meanwhile, in normal concrete, the highest average frequency value of 10214.8 Hz was shown in the BN1 specimen. An extensive evaluation of corroded concrete over 48, 96, and 168 h showed higher FA and SF mixture frequencies. At 168 h, the V2c specimen produced a frequency value of 7712.4 Hz, while BN2 produced a frequency value of 2621.3 Hz. This indicates that a more severe corrosion rate in reinforced concrete can decrease the frequency value. In addition, the amplitude is usually higher in the internal damage area, which is characterized by more significant damage or cracks [16]. Both specimens showed more area noise after being exposed to corrosion than before the measurements. According to Faris et al. [21], corrosion can increase reflected wave amplitude by spreading rust into concrete cracks. At the same time, the presence of chloride and moisture simultaneously significantly attenuates the amplitude and frequency. The combination of FA and SF mixtures has a positive effect in reducing water absorption and chloride permeability, as well as increasing the

https://doi.org/10.31436/iiumej.v26i3.3606

hardness of concrete; the frequency peak is higher than that of normal concrete [2]. The concrete specimens containing fly ash (FA) and silica fume (SF) had fewer internal defects and more uniform wave responses, indicating improved microstructure and overall quality compared to normal concrete.

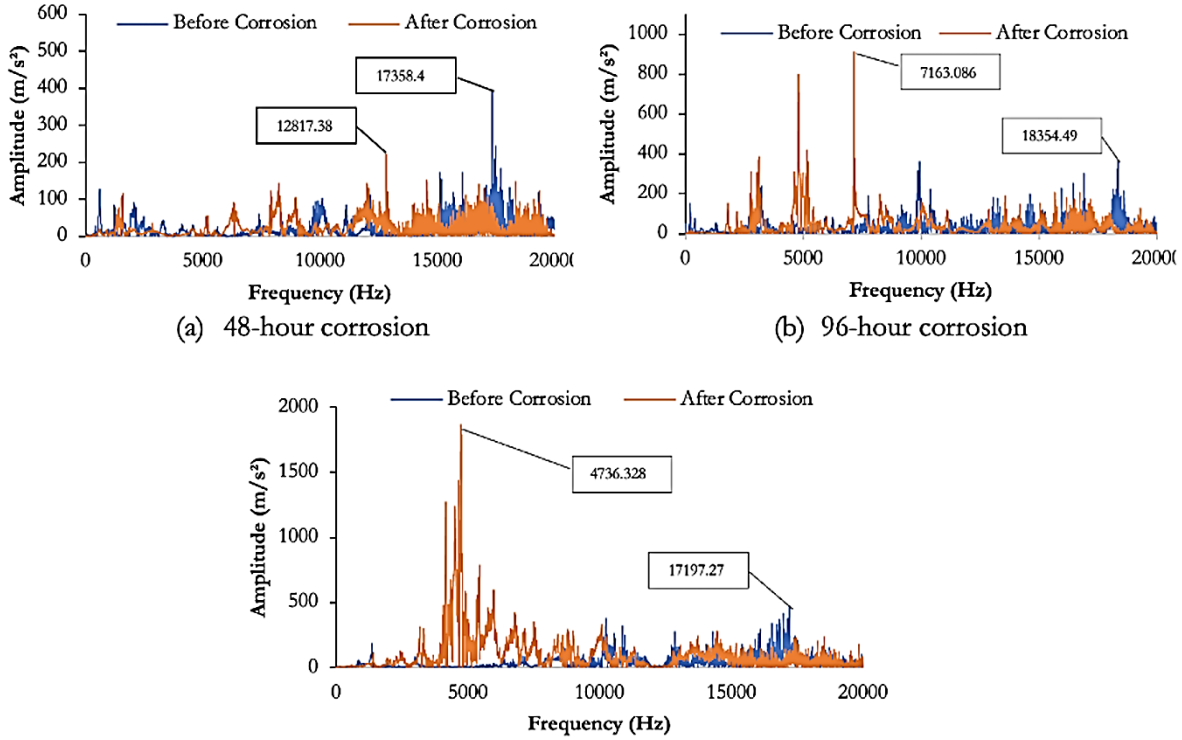

(a) 48-hour corrosion (b) 96-hour corrosion

(c) 168 hours corrosion

Figure 14. Graphs impact of echo before and after corrosion

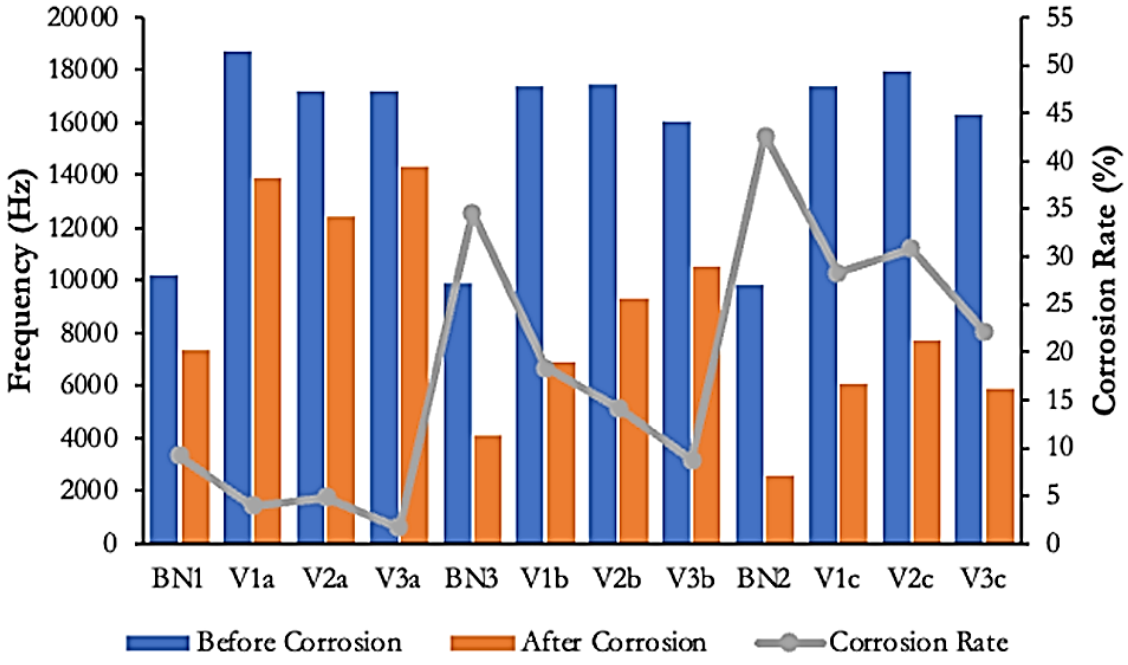

Figure 15. Relationship between frequency value and corrosion rate

https://doi.org/10.31436/iiumej.v26i3.3606

Due to increased density and stiffness from pore refinement and microstructure improvement, concrete with FA and SF mixtures exhibited higher frequencies than normal concrete. This enhancement enabled better wave propagation, resulting in higher resonant frequencies in the impact echo test, which signifies superior material quality and fewer internal defects. In contrast, corroded specimens exhibited a decline in frequency, indicating internal deterioration caused by crack formation, stiffness loss, and increased porosity resulting from corrosion-induced reinforcement expansion. This frequency shift is a reliable indicator of structural damage and degradation within the concrete matrix. The best corrosion resistance was observed for V3. Corrosion significantly affected the frequency values in the impact echo test. The expansion of rust led to crack formation and internal damage, disrupting wave propagation and causing lower, more scattered frequency readings. This decline indicated a loss of concrete stiffness and integrity, highlighting the extent of deterioration caused by corrosion. A greater frequency shift corresponds to higher corrosion levels, as increased internal cracking and stiffness loss further reduce the resonant frequency. This makes frequency shift a reliable indicator for assessing corrosion damage in concrete structures.

3.5. Flexural Strength Results

The bending strength of the reinforced concrete was determined by bending strength testing. The bending strength test was carried out using the three-point bending test method, in which concrete is concentrated on two pedestals with 1-point loading. The bending strength testing was performed after the concrete had been corroded. The results of the flexural strength tests with a mixture of FA and SF variations are shown in Figure 16.

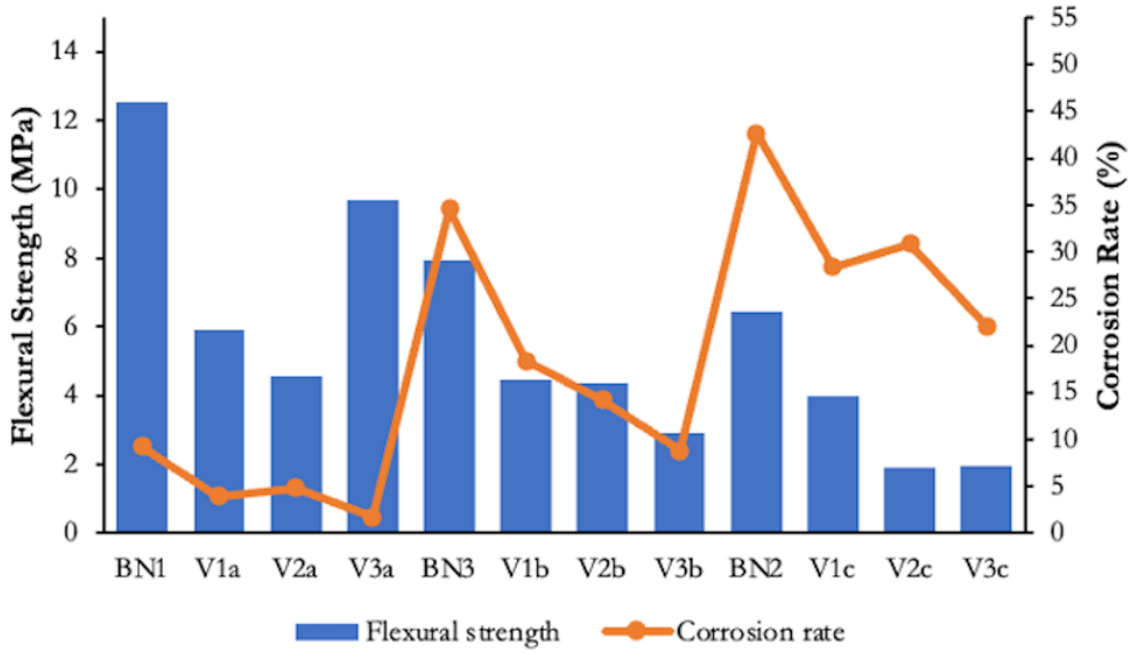

Figure 16. Flexural strength value

Figure 17 shows that the increased corrosion resulted in a decrease in the strength of all specimens. The highest bending strength was observed on the V3 specimen, with a bending strength of 9.69 MPa at a corrosion rate of 1.67%. Meanwhile, at the highest position, BN obtained a bending strength of 12.53 MPa and a corrosion rate of 9.2%. In the 96-hour corroded specimen, the BN specimen at a corrosion rate of 34.6% produced a bending strength of 7.96MPa. Meanwhile, the V2 specimen, at the lowest corrosion rate of 4.79%, had a lower bending strength than BN, with a value of 4.56 MPa. In this case, the corrosion rate did not

https://doi.org/10.31436/iiumej.v26i3.3606

significantly influence the strong bending performance. The best performance was observed for the V3a specimen. The 168-hour corroded specimen showed a different pattern in the V3c specimen, with the lowest bending strength value of 1.93 MPa at a corrosion rate of 22.08%. In contrast, V1c, with a higher corrosion rate of 28.33%, produced a higher flexural strength value of 3.99 MPa.

From the results of this test, it can be concluded that the level of corrosion in each specimen is not the only factor affecting the bending strength of concrete. This is because each specimen exposed to corrosion over time will show a decrease in strength owing to corrosion cracking. The addition of FA and SF can inhibit the corrosion rate, which is characterized by a lower corrosion rate than normal concrete because both decrease the porosity of concrete. However, excessive cement replacement with FA and SF leads to a more significant decrease in strength and water absorption. According to Luo et al. [22], the use of FA is not conducive to increasing the strength and durability of concrete. Still, adding SF can increase the compressive and flexural strengths of concrete. However, as the use of FA and SF increases, the strength of concrete decreases [23]. In this test, the crack pattern of each corroded beam specimen was observed. The appearance of this crack was due to the direction of the crack being perpendicular to the axis of the beam. The bending crack occurred in the middle of the span.

3.6. Crack Patterns

The initial crack in the BN specimen was a bending crack, as shown in Figure 17. Based on the observation of the crack pattern, an initial crack appeared at the bottom of the beam near the load. The cracks widened as the load increased, but no other cracks were observed in the beam. The beam collapsed after deformation with a deflection of 2.604 mm in beam BN1 (48 h corrosion), in beam BN3 2.154 mm (96 h corrosion), and 1.426 mm in beam BN2 (168 h corrosion).

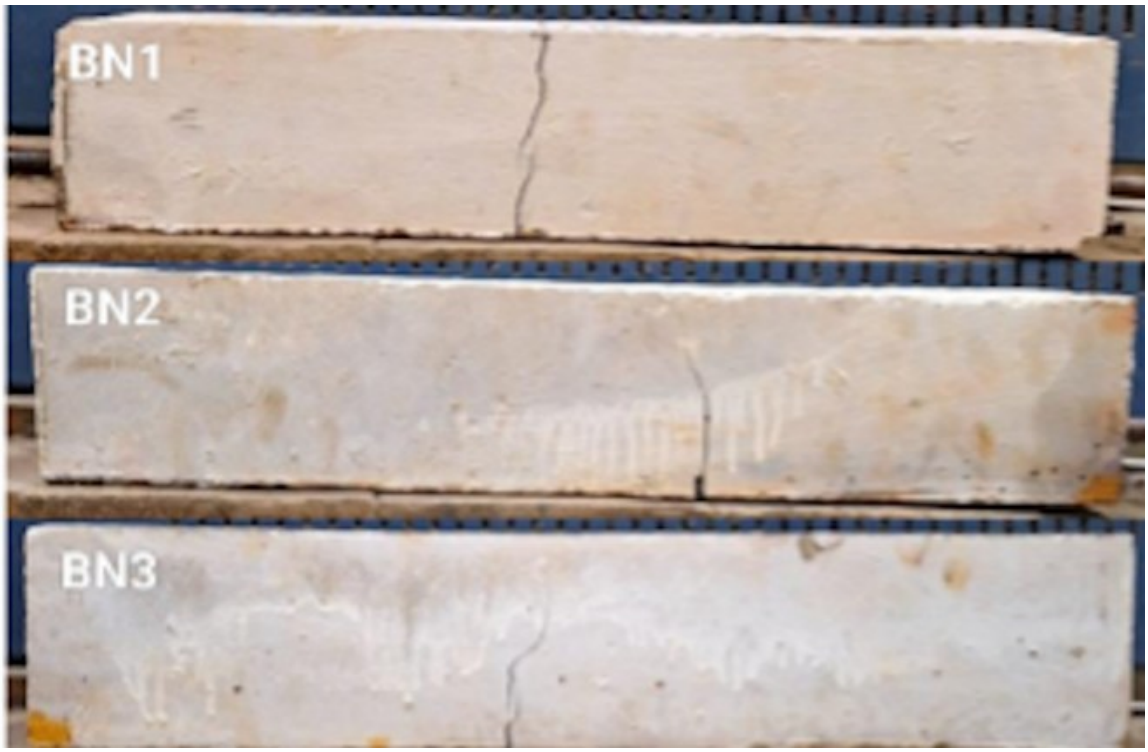

Figure 17. BN beam crack pattern

https://doi.org/10.31436/iiumej.v26i3.3606

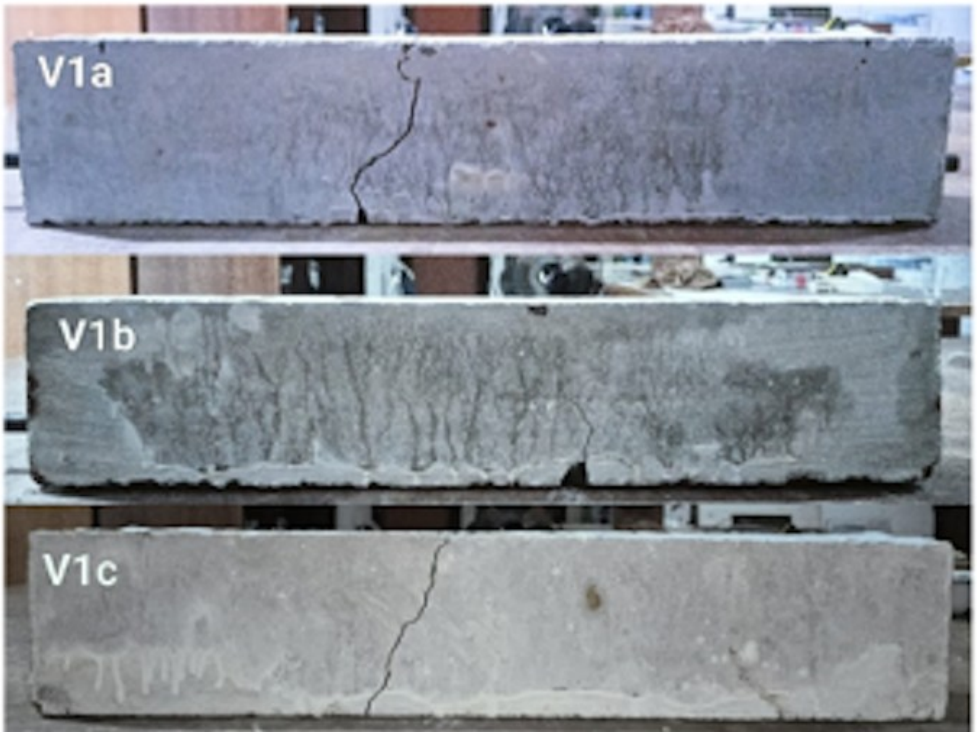

Figure 18. V1 beam crack pattern

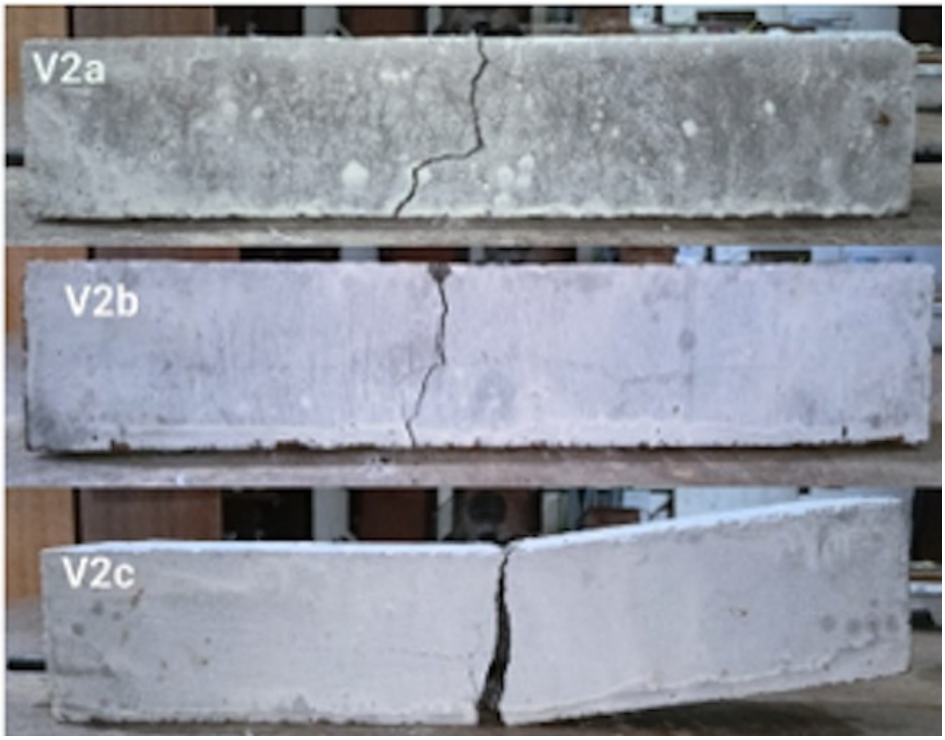

Figure 19. V2 beam crack pattern

The initial crack in the V1 specimen was flexural, as shown in Figure 18. Based on the observation of the crack pattern, an initial crack appeared in the area under the beam close to the load. As the load increased, the cracks widened, and no other cracks were observed along the beams. The beam collapsed after deformation, with a deflection of 3.544 mm on the V1a

https://doi.org/10.31436/iiumej.v26i3.3606

beam (48 h of corrosion), 1.636 mm on the V1b beam (96 h of corrosion), and 1.264 mm on the V1c beam (168 h of corrosion).

The initial crack in the V2 specimen was flexural, as shown in Figure 19. Based on the observation of the crack pattern, an initial crack appeared in the area under the beam close to the load. As the load increased, the cracks widened, and no other cracks were observed along the beams. The beam collapsed after deformation with a deflection of 4.944 mm on the V2a beam (48 h corrosion), on the V2b beam of 2.596 mm (96 h corrosion), and 15.720 mm on the V2c beam (168 h of corrosion).

Figure 20. V3 beam crack pattern

The initial crack in the V1 specimen was flexural, as shown in Figure 20. Based on the observation of the crack pattern, an initial crack appeared in the area under the beam close to the load. As the load increased, the cracks widened, and no other cracks were observed along the beams. The beam collapsed after deformation with a deflection of 5.342 mm on the V3a beam (48 h corrosion), 0.910 mm on the V3b beam (96 h corrosion), and 1.610 mm on the V1c beam (168 h corrosion).

3.7. Microstructure Test Results

SEM testing was performed on specimens corroded for 168 h, and with the best flexural strength, namely, the V1c specimens. The test sample was placed close to the rebar and cut to a maximum size of 1 × 1 × 1 cm. Two test specimens were used for comparison in the analysis: normal concrete samples and concrete containing a mixture of FA and SF. The test results are in the form of photos that show the elements contained in the concrete and can also be seen as the presence of pores or cracks. SEM images are shown in Figure 21.

https://doi.org/10.31436/iiumej.v26i3.3606

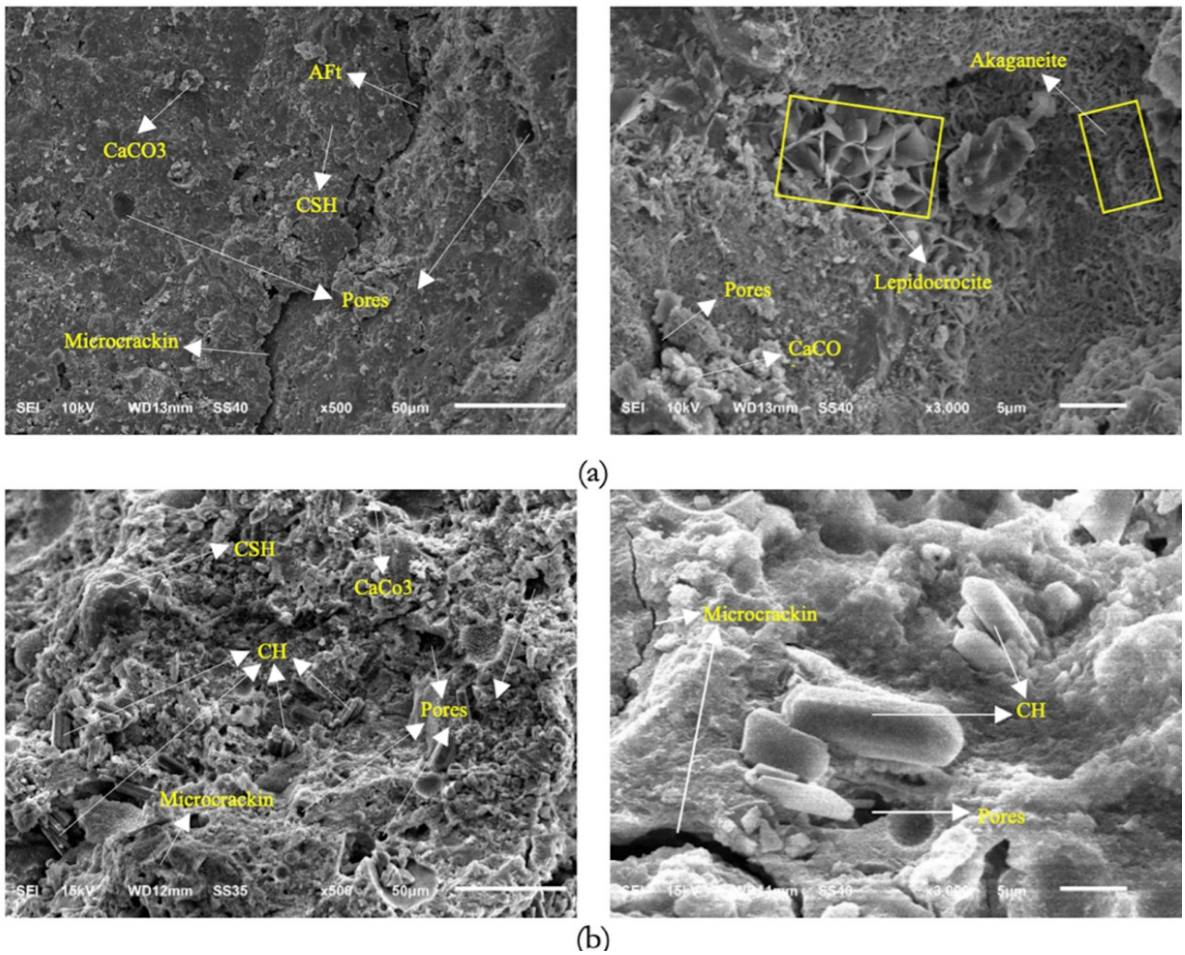

Figure 21. Concrete microstructure (a) BN2 and (b) V1c

In this test, heterogeneous and intermittent distribution of CSH tissue was observed in the V1c specimens, whereas CSH tissues were more homogeneous in the BN2 specimens. This shows that V1c has a weaker structure than that of BN2. The heterogeneous and intermittent distribution of CSH networks on V1c directly leads to a decreased strength compared with BN2, which has a more homogeneous CSH network [24, 25]. The XRD results also showed the identified crystal phase peaks, as shown in Table 7 and Figure 22. XRD testing showed a degree of BN2 of 66.4% for the V1c sample and 72.3%. The degree of crystallinity affects the concrete structure, which is stronger in terms of the concrete's compressive and bending strengths. This suggests that the V1c sample has a composition that is mostly more amorphous than BN2, which can result in lower strength. According to Liu et al. [26], insufficient hydration levels can affect the amount of CSH and the poor crystallinity of the material, thereby reducing the strength of the concrete.

Table 6. Percentage of crystallinity and amorphous Sample

Sample	Crystallinity (5%)	Amorphous (%)
BN2	66.4	33.6
V1c	72.3	27.7

https://doi.org/10.31436/iiumej.v26i3.3606

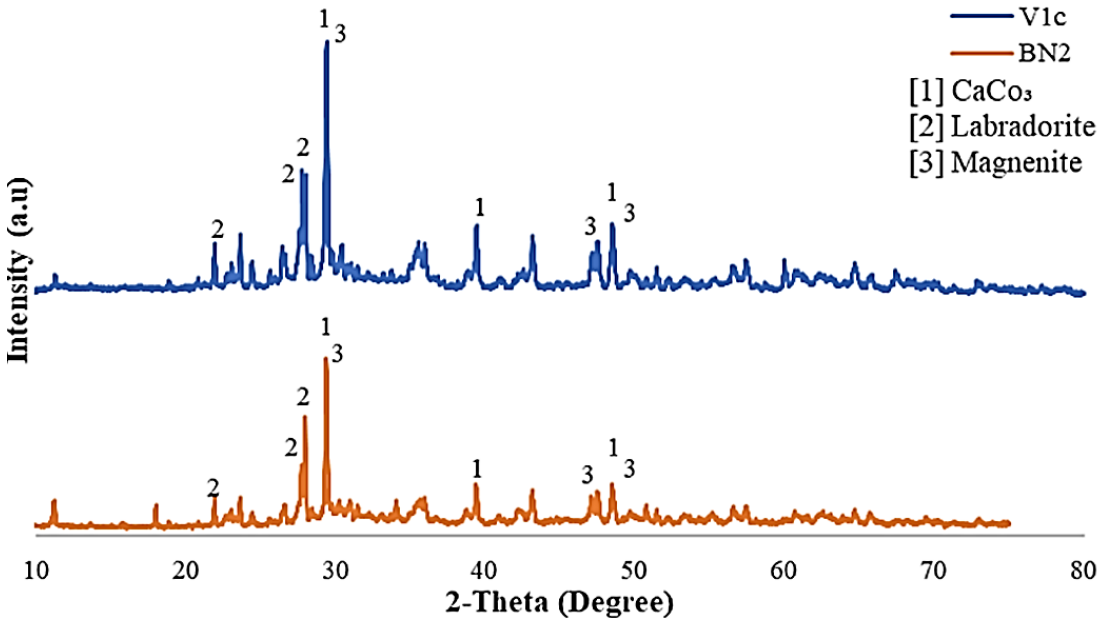

Figure 22. XRD analysis graph

1. CONCLUSIONS

Based on the experimental results and data analysis, the corrosion evaluation of fly ash (FA) and silica fume (SF) concrete using non-destructive testing (NDT) methods reveals several key findings. The compressive strength of concrete generally declined as the percentage of cement replacement with FA and SF increased, with SF in particular contributing to higher water absorption, lower workability, and reduced strength. Over time, all specimens exhibited a decrease in flexural strength due to corrosion-induced cracking, which was further influenced by mechanical degradation resulting from weaker grain adhesion and delayed pozzolanic reactions compared to conventional cement hydration. Nonetheless, the inclusion of FA and SF effectively inhibited the corrosion rate, as confirmed by resistivity and impact echo analyses. The FA and SF concrete samples demonstrated higher corrosion resistance than normal concrete, with pre-corrosion resistivity values ranging from 37–254 kΩ·cm (very low corrosion risk), compared to 21–37 kΩ·cm for normal concrete (low corrosion risk). Additionally, peak frequency values from impact echo testing were notably higher in FA and SF mixes (16,000–18,000 Hz) than in normal concrete (8,000–12,000 Hz), indicating denser internal structures. Both resistivity and impact echo values declined with prolonged exposure to corrosion acceleration. Among all mixes, the V3 specimen, containing 30% FA and 15% SF, exhibited the best overall corrosion performance, balancing mechanical integrity and corrosion resistance most effectively.

ACKNOWLEDGEMENT

This work was supported by the Ministry of Education, Culture, Research, and Technology (Indonesia), Grant number 107/E5/PG.02.00.PL/2024, and by Universitas Muhammadiyah Yogyakarta.

REFERENCES

[1] Nindhita KW, Zaki A, Zeyad AM. (2024) Effect of Bacillus Subtilis Bacteria on the mechanical properties of corroded self-healing concrete. Frattura ed Integrita Strutturale, 18(68):140-58.

[2] Zaki A, Fikri MA, Wibisono CA, Rosyidi SAP. (2023) Evaluating Pre-Corrosion and Post-Corrosion of Oil Palm Shell Concrete with Non-Destructive Testing. Key Engineering Materials, 942:137-62.

[3] Zaki A, Chai HK, Aggelis DG, Alver N. (2015) Non-destructive evaluation for corrosion monitoring in concrete: A review and capability of acoustic emission technique. Sensors (Switzerland), 15(8):19069-101.

[4] Saraswathy V, Muralidharan S, Thangavel K, Srinivasan S. (2003) Influence of activated fly ash on corrosion-resistance and strength of concrete. Cement and Concrete Composites, 25(7):673-80.

[5] Baltazar-Zamora MA, D MB, Santiago-Hurtado G, Mendoza-Rangel JM, Gaona-Tiburcio C, Bastidas JM, et al. (2019) Effect of Silica Fume and Fly Ash Admixtures on the Corrosion Behavior of AISI 304 Embedded in Concrete Exposed in 3.5% NaCl Solution. Materials (Basel), 12(23):4007.

[6] Adamu M, Mohammed BS, Liew MS. (2018) Mechanical properties and performance of high volume fly ash roller compacted concrete containing crumb rubber and nano silica. Construction and Building Materials, 171:521-38.

[7] ACI. (1991) Standard Practice for Selecting Proportions for Normal, Heavyweight, and Mass Concrete. ACI Committe, 1-38.

[8] AASHTO. (2014) AASHTO TP 95-14 : Standard Test Method for Surface Resistivity of Concrete's Ability to Resist Chloride Ion Penetration. Washington, D.C: AASHTO.

[9] ASTM. (2022) C1383 : Standard Test Method for Measuring the P-Wave Speed and the Thickness of Concrete Plates Using the Impact-Echo Method. West Conshohocken, PA: ASTM International, 1-11.

[10] ASTM. (1985) ASTM STP866-EB : Laboratory Corrosion Tests and Standards. ASTM International, 1-640.

[11] Hong S, Zheng F, Shi G, Li J, Luo X, Xing F, et al. (2020) Determination of impressed current efficiency during accelerated corrosion of reinforcement. Cement and Concrete Composites, 108:103536.

[12] Singh M, Siddique R. (2015) Effect of Low-Calcium Coal Bottom Ash as Fine Aggregate on Microstructure and Properties of Concrete. ACI Materials Journal, 112(5), 693-703.

[13] Williams KC, Balamuralikrishnan R. (2023) Strength prediction and correlation of concrete by partial replacement of fly ash & silica fume. Advances in Concrete Construction,16(6):317-25.

[14] BSN. (2011) SNI 1974:2011: Cara uji kuat tekan beton dengan benda uji silinder (How to test the compressive strength of concrete using cylindrical test specimens). Jakarta: Badan Standarisasi Nasional, 1-20.

[15] Mermerdaş K, İpek S, Anwer AM, Ekmen Ş, Özen M. (2021) Durability performance of fibrous high-performance cementitious composites under sulfuric acid attack. Archives of Civil and Mechanical Engineering, 21(4):147.

[16] Alhawat M, Khan A, Ashour A. (2020) Evaluation of steel corrosion in concrete structures using impact-echo method. Advanced Materials Research, 1158:147-64.

[17] Gómez-Luna G, López-Calvo H, Bremner T, Fajardo-San Miguel G, Castro-Borges P, Montes-García P. (2023) Assessment of corrosion prevention methods for steel reinforcement embedded in concrete exposed to a natural marine environment. Construction and Building Materials, 385:131514.

[18] Zaki A, Rahayu H, Nugraha DA, Rosyidi SAP, Kencanawati NN, Fonna S, editors. (2024) Resistivity Method Evaluation of Corroded OPS-Concrete. E3S Web of Conferences; EDP Sciences.

[19] Sadrmomtazi A, Tahmouresi B, Kohani Khoshkbijari R. (2018) Effect of fly ash and silica fume on transition zone, pore structure and permeability of concrete. Magazine of Concrete Research, 70(10):519-32.

[20] Panjehpour M, Ali AAA, Demirboga R. (2011) A review for characterization of silica fume and its effects on concrete properties. International Journal of Sustainable Construction Engineering and Technology, 2(2).

[21] Faris N, Zayed T, Abdelkader EM, Fares A. (2023) Corrosion assessment using ground penetrating radar in reinforced concrete structures: Influential factors and analysis methods. Automation in Construction, 156:105130.

[22] Luo S, Liang W, Wang H, Wang W, Zou R. (2021) Durability evaluation of concrete with multiadmixtures under salt freeze-thaw cycles based on surface resistivity. Advances in Materials Science and Engineering, 2021:1-18.

[23] Wang J, Che Z, Zhang K, Fan Y, Niu D, Guan X. (2023) Performance of recycled aggregate concrete with supplementary cementitious materials (fly ash, GBFS, silica fume, and metakaolin): Mechanical properties, pore structure, and water absorption. Construction and Building Materials, 368:130455.

[24] Hlobil M, Sotiriadis K, Hlobilova A. (2022) Scaling of strength in hardened cement pastes-Unveiling the role of microstructural defects and the susceptibility of CSH gel to physical/chemical degradation by multiscale modeling. Cement and Concrete Research, 154:106714.

[25] Chen J, Li Z, Jin X. (2017) Morphological effect of C–S–H gel on the elastic behaviour of early-age cement-based materials. Magazine of Concrete Research, 69(12):629-640.

[26] Liu B, Zhang Q, Zhao Y, Huan D, Liu X. (2023) Influence of high altitude on the strength of aerated concrete. RSC advances, 13(17):11762-11770.